

# A Real-Time QRS Detection Method Based on Phase Portraits and Box-Scoring Calculation

Zhongjie Hou, Yonggui Dong, Jinxi Xiang, Xuewu Li, and Bin Yang

**Abstract**—In order to detect the QRS complexes locally in the microcontroller-based embedded system, a novel algorithm with lower computation burden is proposed by phase space reconstruction and box-scoring calculation. The method depends on the geometrical property of the ECG signal phase portraits. According to the time-delay method, one segment of the sampled 1-D ECG signal is embedded into a 2-D phase space. The phase space is divided into  $2^M \times 2^M$  grids, and each grid is called a box. The box gridding is implemented by numerically truncating the high  $M$ -bits from the digital data. The phase portraits of the sampled ECG signal in the phase space are therefore divided by these boxes. Since the trajectory points corresponding to the R-waves are located relatively far away from the diagonal line, boxes that crossed by the trajectory are flagged and valued according to its distance to the diagonal line. Correspondingly, the box-scoring of the ECG segment is obtained by summarizing the values of the flagged boxes. The location of the R-waves can then be found by finding peak values in the box-scoring time series. The proposed algorithm is suitable for real-time QRS complex detection in microcontroller-based wearable ECG acquisition devices.

**Index Terms**—Electrocardiograph, phase portraits, phase space reconstruction, box-scoring, QRS complex detection.

## I. INTRODUCTION

WITH the development of sensor technology and mobile Internet, wearable devices that can conveniently obtain basic physiological parameters of human body have become an important research area [1], [2]. Cardiovascular disease is one of the main diseases that endanger human health. Wearable devices that can measure electrocardiogram (ECG) signals especially the heart rate variability (HRV) are becoming powerful tools for self-monitoring in daily life [3]. HRV is highly related to stress, anxiety, diabetes, hypertension, fatigue, and depression symptoms [4], [5]. Different from the clinical ECG monitor, wearable ECG devices are used in daily life. Relatively larger measurement error is acceptable for some health care applications [6]. The acceptance of the wearable devices depends on user-awareness, as well as clinician and patient acceptance. In addition to the detection accuracy,

Manuscript received December 27, 2017; accepted March 3, 2018. Date of publication March 9, 2018; date of current version April 9, 2018. This work was supported in part by the National Natural Science Foundation of China under Grant 61671270. The associate editor coordinating the review of this paper and approving it for publication was Prof. Aime Lay-Ekuakille. (*Corresponding author: Yonggui Dong*)

Z. Hou, Y. Dong, J. Xiang, and B. Yang are with the State Key Laboratory of Precision Measurement Technology and Instruments, Department of Precision Instrument, Tsinghua University, Beijing 100084, China (e-mail: dongyg@mail.tsinghua.edu.cn).

X. Li is with the School of Mechanical, Electronic and Control Engineering, Beijing Jiaotong University, Beijing 100044, China.

Digital Object Identifier 10.1109/JSEN.2018.2812792

the energy sustainability and algorithm complexity should be considered [7], [8].

The QRS complex detection and heart rate (HR) calculation are the primary tasks of ECG signal processing algorithms in wearable ECG devices. Many QRS detection algorithms have been reported as reviewed in [9]. The most classical QRS complex detection algorithm was introduced by Pan and Tompkins [10]. It is designed based on band-pass filter and differential method. In case of that the ECG signal is weakly disturbed by the noise, the QRS complex detection can be implemented real-timely and relatively satisfied performance can be obtained. Some modified form of pan Tompkins algorithms can be found in [11] and [12]. The wavelet transform is widely used in QRS complex detection. Ghaffari *et al.* [13] defined the dominant rescaled wavelet coefficients to detecting the QRS complex. Jorge *et al.* [14] and Sahoo *et al.* [15] combined Hilbert and Wavelet transforms and an adaptive threshold technique to detect the QRS complex of ECG signals. The quadratic filter was employed on ECG signals to enhance the QRS detection rate [16]. These methods can significantly improve the QRS complex detection accuracy, however, the cost is larger calculation burden.

Lee *et al.* [17] and Cvikel *et al.* [18] used the embedding method to transfer the one-dimensional ECG signal to the two-dimensional phase space. By calculating the polygon area of the phase portraits of the ECG signal, the baseline drift and other noisy interference can be suppressed. To detect the ventricular fibrillation (VF), Amann *et al.* [19], Sarvestani *et al.* [20], and Roopaei *et al.* [21] gridded the phase space into several grids, and count the boxes visited by the phase portraits of ECG signal.

Inspired by the idea of polygon area calculation [17], [19] and gridding partition methods [19]–[21], a novel real-time QRS complex detection algorithm, which is termed as box-scoring calculation, is proposed in this paper. The phase space is divided into low-resolution  $2^M \times 2^M$  boxes. Boxes that crossed by the trajectory are flagged and valued according to its distance from the diagonal line. Then the box-scoring is obtained by summarizing the values of the flagged boxes. The R-wave detection can be done by finding peaks in the box-scoring time series. Since only addition and subtraction are needed for box-scoring calculation, a fast QRS complex detection can be implemented real-timely in microcontroller-based wearable ECG acquisition devices.

## II. QRS COMPLEX DETECTION ALGORITHM

The embedding method [22]–[24] is a common method for dealing with time series. For a sampled one-dimensional

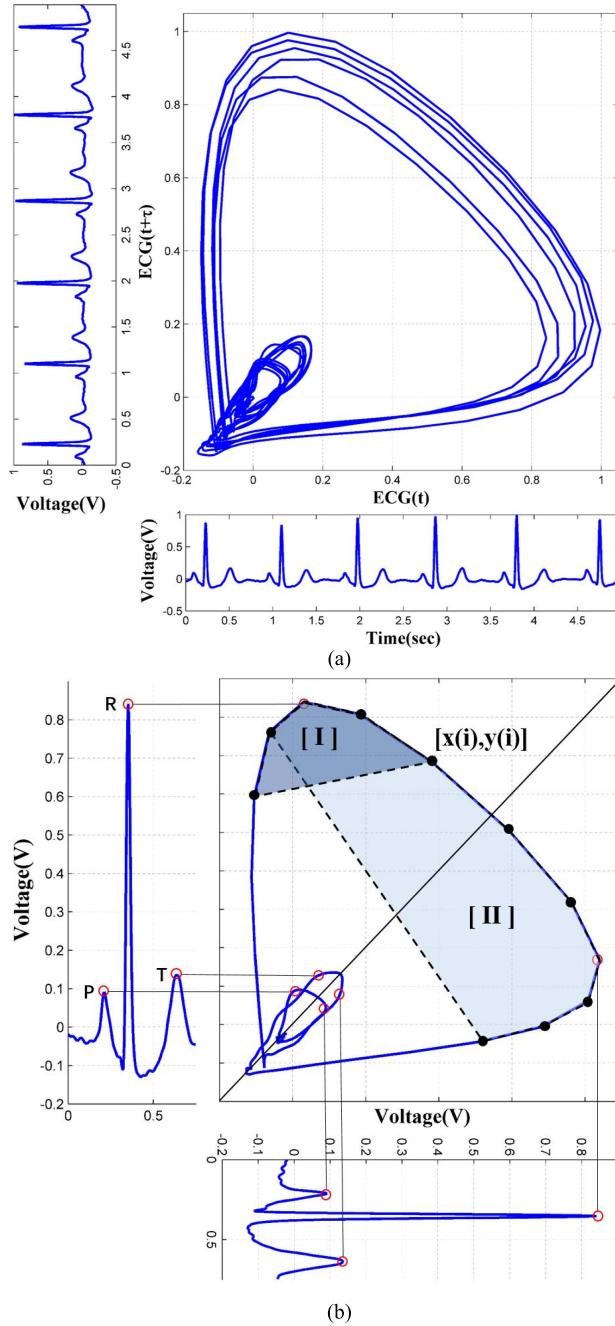


Fig. 1. Phase portraits of the ECG signal ( $\tau = 20ms, m = 2$ ). (a) ECG signals and the corresponding phase portraits. (b) ECG feature points on phase portraits (polygon I:  $n = 5$ , polygon II:  $n = 10$ ).

time series  $X, X = (x_1, x_2, x_3, \dots, x_N)$ ,  $m$ -dimensional delay vectors  $p(i), p(i) = (x_i, x_{i+\tau}, x_{i+2\tau}, \dots, x_{i+(m-1)\tau})$  are obtained by the embedding method. The parameter  $m$  is the mapping dimension of the phase space. According to that reported by Lee *et al.* [17], two dimension ( $m = 2$ ) is satisfactory to extract the feature of the ECG signal. Another parameter  $\tau$  is the time delay which can be chosen by fill-factor [25] or mutual information [26]. The parameter  $\tau$  is set to 20ms in our cases, and it is consistent with the experimental results in [17] and [18]. As an example, Fig.1 shows the reconstructed phase portraits of the ECG signal by  $\tau = 20ms$

and  $m = 2$ . The waveforms and the phase portraits of the ECG signal is shown in Fig.1a. Particularly, the phase portrait of one heart beat cycle is given in Fig.1b. The location of the feature points, such as P, R and T fiducial points, are marked on the ECG waveforms and the corresponding phase portrait.

In order to stand out the QRS complex features, Lee *et al.* [17] and Cvikel *et al.* [18] calculated the polygon area (the shadowed area in Fig.1b) by the followed equation.

$$\text{PA} = \frac{1}{2} |x(1)y(2) - y(1)x(2) + \dots + x(n-1)y(n) - y(n-1)x(n) + x(n)y(1) - y(n)x(1)| \quad (1)$$

Where  $[x(i), y(i)], 1 \leq i \leq n$  is the point coordinates of trajectory in the two-dimensional plane,  $n$  is the number of points for area calculation. Practically, the  $n$  equals to the length of the computational sliding window of the ECG signal. It can be inferred from Fig.1b (I:  $n = 5$ , II:  $n = 10$ ) that, if  $n$  is too small, two peaks corresponding to one R-wave will be obtained from PA calculation since the same R-point appears twice in the phase portrait. The selection of  $n$  will be discussed in Section III. Because the multiplication of floating-point numbers is included, the computational cost is relatively large. In order to detect the VF, Amann *et al.* [19] proposed another method. They divided the phase space into hundreds of boxes and counted the number of boxes visited by the trajectory of ECG signal. Since the phase portraits of the typical VF signal will fill more area of the phase space, a measure  $d$  for VF detection, defined by Eq.2, is used as a parameter for VF detection.

$$d = \frac{\text{Number of visited boxes}}{\text{Number of all boxes}} \quad (2)$$

If  $d$  is higher than a certain threshold  $d_0$ , the corresponding ECG episode is classified as VF. Because almost no floating-point calculation is engaged, this method is easily implemented and can work real-timely.

Inspired from the above mentioned methods, a new method for QRS complex detection, which we termed as box-scoring calculation, is proposed as follows.

The two-dimensional phase space is partitioned into  $2^M \times 2^M$  grids and each grid is called a box. This gridding procedure can be done by numerically truncating the high  $M$ -bits from the digital data (Fig.2a). For example, if the ECG signal is sampled at 8-bits resolution, the embedded space portrait shown in Fig.2b can be transferred to a  $2^6 \times 2^6$  grids by simply truncating the high 6-bits of the original data (Fig.2c).

It can be seen from Fig.1b that, phase portraits corresponding to the R-wave are located relatively far away from the diagonal line. On the contrary, those points of the other ECG features are concentrated to a restricted region near the diagonal line. Therefore, the distance from point to the diagonal line can be used as an indicator for discriminating the R-wave from the other ECG features. Since the diagonal is a 45-degree line, the distance can be obtained simply by differential operation. As shown in Fig.3 ( $M = 4$ , to give a clear illustration), if one  $\text{box}_{[u(i), v(i)]}$  is crossed by the signal trajectory, it is flagged and its value is given by its distance

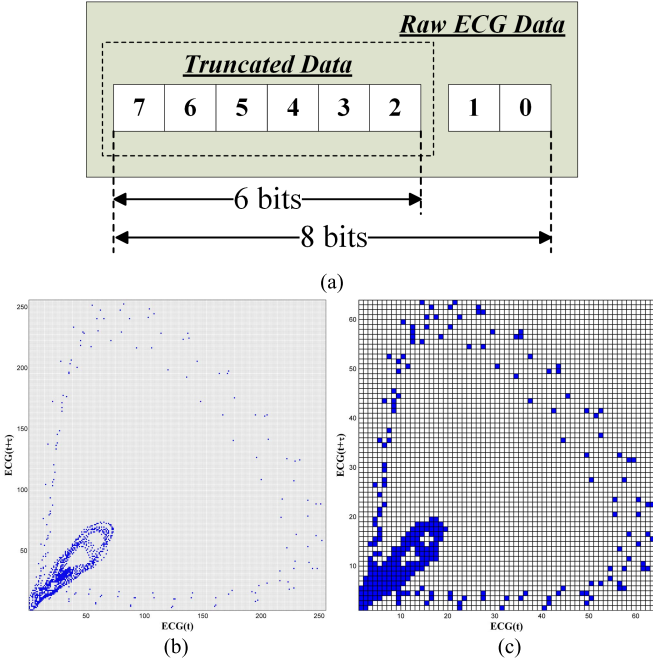


Fig. 2. Gridding procedure. (a) Numerically truncating. (b) Original phase portraits ( $M = 8$ ). (c) Gridded phase portraits ( $M = 6$ ).

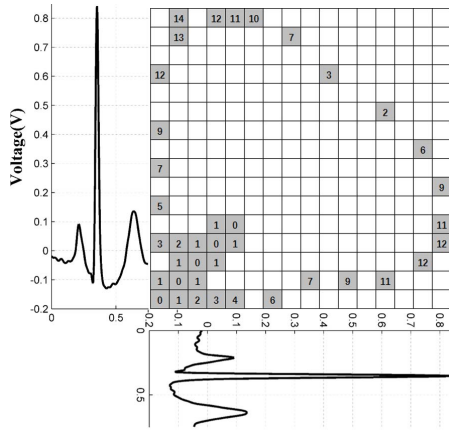


Fig. 3. An example of the gridded phase portraits ( $16 \times 16$ ).

from the diagonal line.

$$dis(i) = |u(i) - v(i)|, \quad 1 \leq u(i), v(i) \leq 2^M \quad (3)$$

Where  $[u(i), v(i)]$  is the coordinates of the  $box_{[u(i), v(i)]}$  in the  $2^M \times 2^M$  gridded two-dimensional space.

When an  $n$ -point length sliding window is applied along the sampled ECG time series, the phase portrait of one segmented signal within one window will appear as a collection of flagged boxes in the gridded space. The box-scoring (BS) of the segmented signal can be calculated by summarizing the values of the flagged  $n$ -boxes.

$$BS(i) = \sum_{k=0}^{n-1} dis(i-k), \quad n \leq i \leq N \quad (4)$$

Where  $N$  is the length of the whole ECG signal time series. Knowing that the phase portraits are constructed from

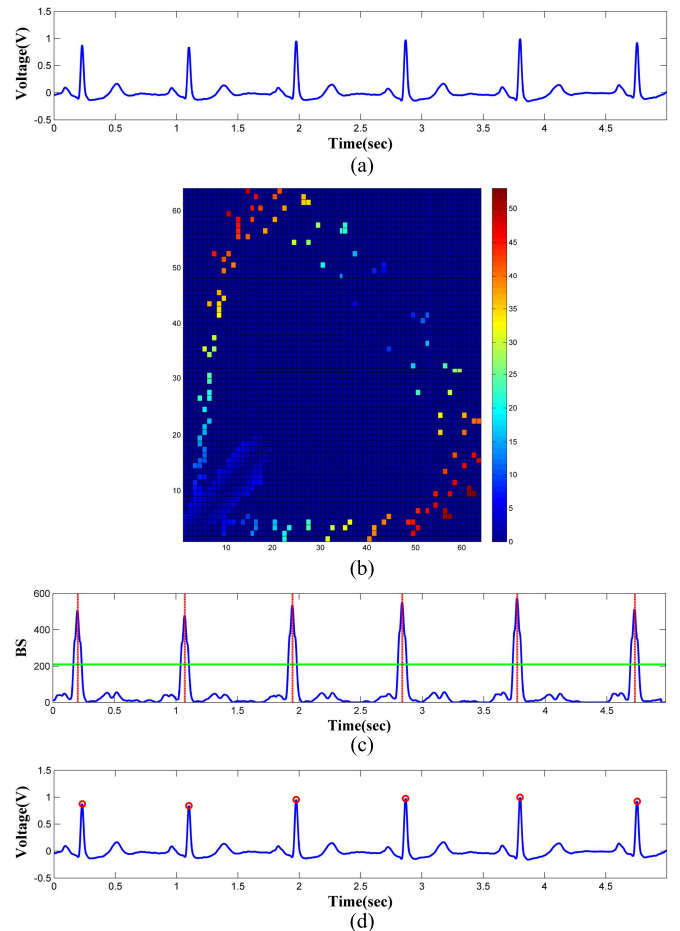


Fig. 4. Box-scoring calculation. (a) ECG signal. (b) Weight value of the flagged boxes. (c) Box-scoring time series. (d) QRS complex detection results.

time series  $x_i$  by delay method, i.e.,  $y_i = x_{i+delay\_point}$ , the box-scoring (BS) calculation can be programmed as follows.

$$BS(i) = |x(i-n+1) - y(i-n+1)| + |x(i-n+2) - y(i-n+2)| + \dots + |x(i) - y(i)| \quad (5)$$

One example is given in Fig.4. A five second ECG signal, sampled by 250Hz and 12-bits resolution, is shown in Fig.4a.

Step 1: Gridding and box assignment. The original ECG signal is transferred to 6-bits resolution by the truncating the high 6-bits of the original 12-bits data. Then, it is mapped to the two-dimensional space by phase portraits reconstructing ( $\tau = 20ms, m = 2$ ), and gridded into  $2^6 \times 2^6$  boxes. The values of all the flagged boxes are calculated (Eq.4) and shown in Fig.4b.

Step 2: Box-scoring calculation. The BS time series is calculated by Eq.5 ( $n = 10$ ). It can be seen from Fig.4c that peaks produced by the QRS complexes can clearly be distinguished from the other features.

Step 3: Peak detection. The local maximum peaks of the BS time series are located. The set of amplitude and timing criteria used in peak detection algorithm is similar to that of [10] and [18]. In our cases, the block length of the sliding window is set as 1.5 second, and the amplitude threshold is set as the 3.8 times of the average values of the box-scoring in

the block (the green horizontal line shown in Fig.4c). Finally, the QRS complex detection results are obtained according to the peak detection results of the BS time series (Fig.4d). The main steps of this method are presented in Algorithm 1.

#### Algorithm 1 Box-Scoring Calculation

```

Input: A sequence of ECG signal X,  $X = (x_1, x_2, x_3, \dots, x_N)$ 
1:  $X \leftarrow \text{Gridding}(X)$  # Gridding process
2: for  $i = 1$  to  $N - \text{delay\_point}$  do
3:    $P(x_i, y_i) \leftarrow (x_i, x_{i+\text{delay\_point}})$  # 2D Embedding
4:   if  $i \geq n$  then
5:     for  $k = 0$  to  $n - 1$  do
6:        $\text{BS}(i) \leftarrow \text{BS}(i) + |x_{i-k} - y_{i-k}|$  # BS calculation
7:     end for
8:   else if  $i < n$  then
9:      $\text{BS}(i) \leftarrow 0$ 
10:  end if
11: end for
12: PEAKS  $\leftarrow$  Find the peak points on the BS time series
      according to [10, 18]
13: ECG_PEAKS  $\leftarrow$  Fix the PEAKS on the ECG signal X

```

### III. RESULTS AND DISCUSSION

#### A. Parameter Selection

The length of the sliding window  $n$  is the number of points for box-scoring calculation. Just like that of polygon area calculation [17], [18], the selection of  $n$  will affect the waveform of the box-scoring time series. The phase portraits of the R-wave is relatively symmetrical (see Fig.1b). When  $n$  is small, say  $n = 5$ , one R-wave will result in two peaks in the calculated BS time series (Fig.5b). With larger  $n = 10$  and  $n = 15$ , clear peaks can be obtained in the BS time series as shown in Fig.5c and Fig.5d. When  $n$  is 20 and 25 (Fig.5e,f), the local maxima corresponding to the R-wave is blunted. In our case (250Hz sampling frequency), the  $n$  is set as 10.

$M$  is another important parameter. The number of boxes is determined by this parameter. A larger  $M$  will retain more details of the signal, and therefore increase the accuracy of the algorithm. However, with the increase of  $M$ , the calculation burden is also increased. The range of  $M$  is limited by the full scale voltage range and the QRS peak amplitude. The resolution of the gridded ECG signal is defined as:

$$\text{Re} = \frac{V_{fsr}}{2^M} \quad (6)$$

where  $V_{fsr}$  is the full scale voltage range. The relative amplitude of the QRS peak must be greater than the resolution. Let  $\overline{V_R}$  represents the average of the relative amplitude of the QRS peak, thus the minimum  $M$  is calculated as:

$$M_{\min} > \log_2 \frac{V_{fsr}}{\overline{V_R}} \quad (7)$$

The recordings of the MIT/BIH arrhythmia database were digitized at 360 samples frequency with 11-bits resolution over

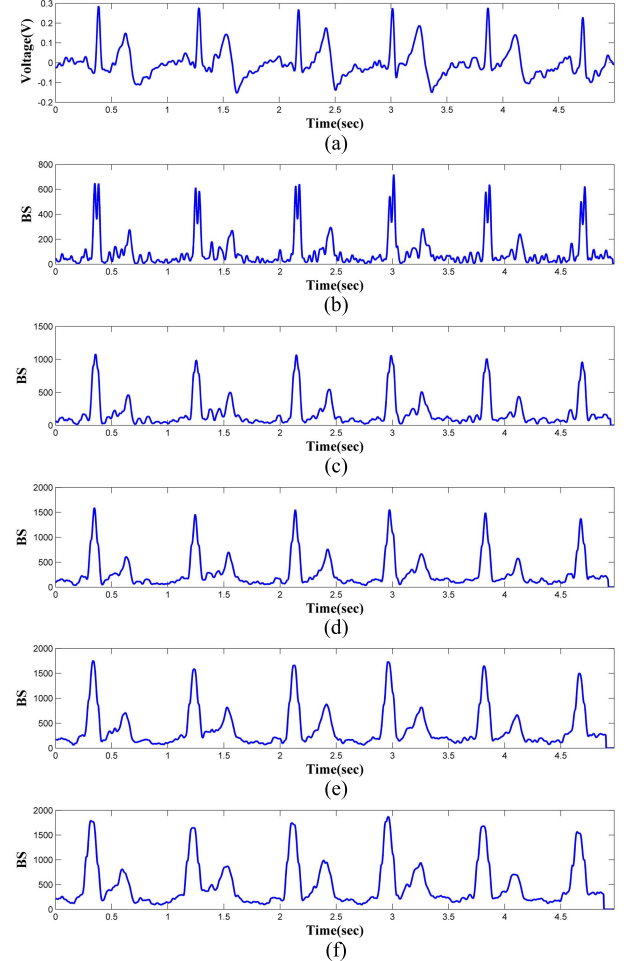


Fig. 5. Box-scoring time series at different  $n$ . (a) raw ECG signal. (b)  $n = 5$ . (c)  $n = 10$ . (d)  $n = 15$ . (e)  $n = 20$ . (f)  $n = 25$ .

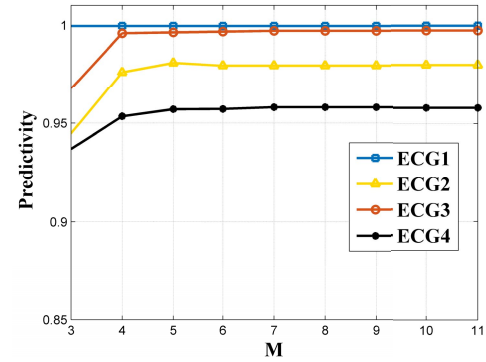


Fig. 6. QRS complex detection results under different  $M$ .

a 10mV range [27]. The average amplitude of the QRS peak is about 1.7mV. The calculated result of the  $M_{\min}$  is 3. Simulations are done to find a reasonable  $M$  by four segments of ECG signals. Each segment of ECG signal is randomly chosen from MIT/BIH arrhythmia database (recordings: No.100, No.113, No.101 and No.203). The duration of each ECG signal is 10 minutes, and each signal contains different levels of noise. The QRS detection results with different  $M$  are shown in Fig.6. The predictivity rises with the increase of  $M$  ( $M < 6$ ). In cases

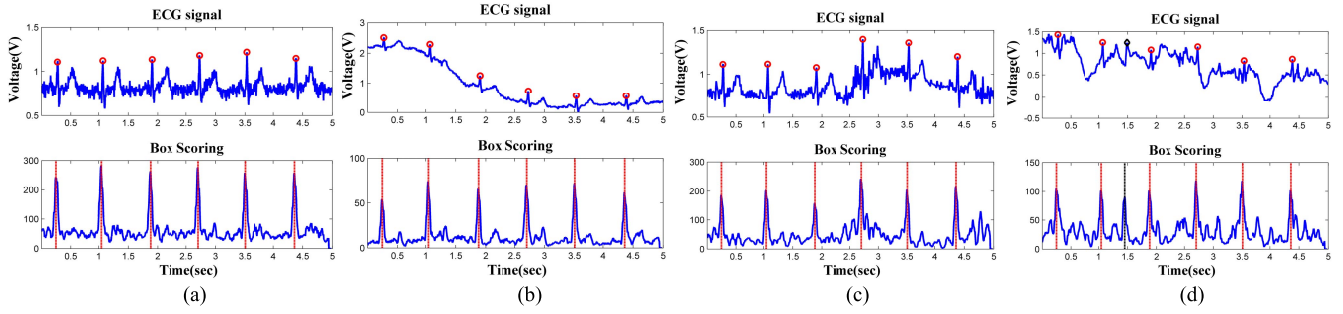


Fig. 7. Box-scoring calculation under different kinds of interference. (a) White noise. (b) Baseline wander. (c) Muscle artifacts. (d) Electrode movements.

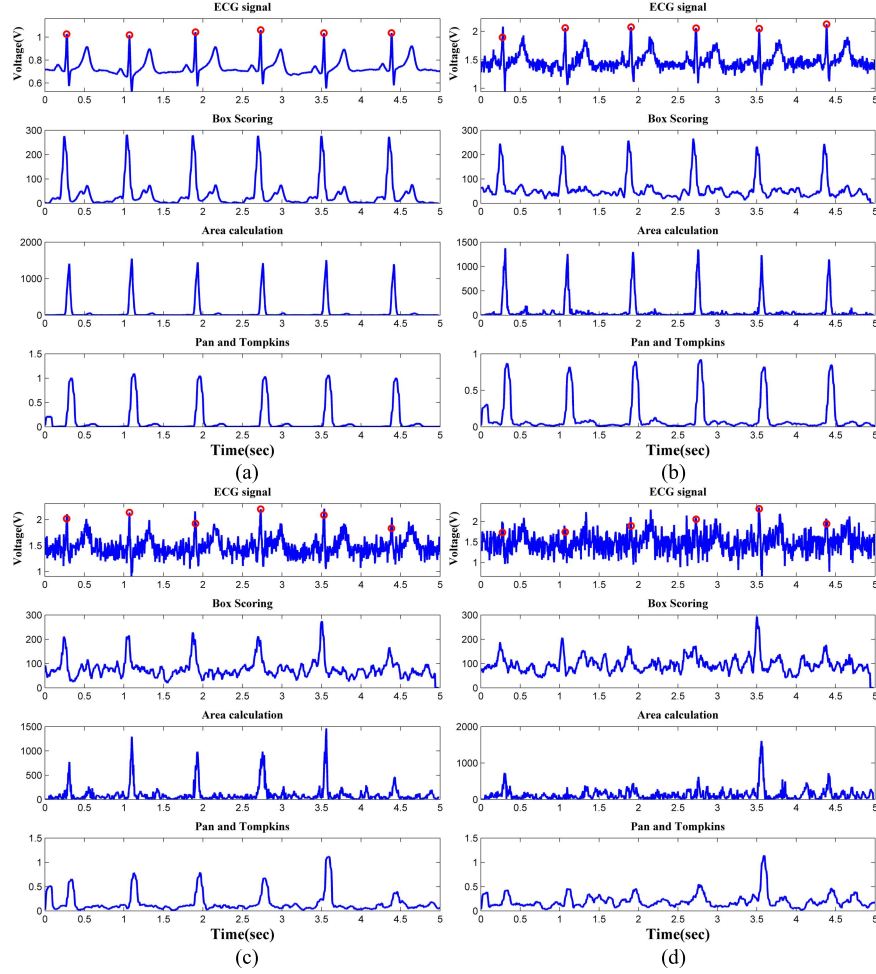


Fig. 8. Box-scoring calculation algorithm compared with others. (a) Raw ECG signal. (b) SNR=10dB. (c) SNR=5dB. (d) SNR=0dB.

of  $M \geq 6$ , the predictivity stay in a relative stable level. Considering the computation efficiency and QRS detection accuracy, the  $M$  is set as 6.

### B. Robust Evaluation

In order to evaluate the robustness of the box-scoring calculation, simulations under different kinds of interference are carried out with MATLAB (R2014a). The results are given in Fig.7. As shown in Fig.7a, a simulated noisy ECG signal (SNR=10dB) is generated by adding random white noise to an ideal ECG signal. Even though there are burrs, the QRS

complex features can be clearly detected. In cases of baseline wander and muscle artifacts, the QRS complex features are still distinguished from other waveform features (Fig.7b, c). However, when the electrode movements interference is added into the ECG signal, the local disordered waveforms have high amplitudes in the BS time series, and false positive (FP) detections will appear (the black diamond shown in Fig.7d).

The performance of the box-scoring calculation is compared with that of polygon area calculation [17], [18] as well as Pan and Tompkins [10]. The white noise is added into the ideal ECG to generate signals with different SNRs, and the processed results are shown in Fig.8. In cases of higher

TABLE I  
RESULTS OF THE BOX-SCORING QRS COMPLEX DETECTION ALGORITHM  
USING THE MIT/BIH ARRHYTHMIA DATABASE

REC	Total	TP	FN	FP	Se(%)	P(%)
100	2273	2272	0	1	100.00	99.96
101	1873	1862	6	5	99.68	99.73
102	2186	2186	0	0	100.00	100.00
103	2084	2084	0	0	100.00	100.00
104	2235	2219	16	21	99.28	99.06
105	2578	2558	20	41	99.22	98.41
106	2096	2094	2	0	99.90	100.00
107	2138	2136	2	0	99.91	100.00
108	1763	1752	11	9	99.38	99.49
109	2519	2517	2	14	99.92	99.44
111	2124	2117	7	8	99.67	99.62
112	2549	2539	10	0	99.61	100.00
113	1795	1795	0	34	100.00	98.11
114	1885	1876	9	22	99.52	98.83
115	1960	1952	8	0	99.59	100.00
116	2401	2395	6	18	99.75	99.25
117	1538	1535	3	0	99.80	100.00
118	2298	2296	2	2	99.91	99.91
119	2010	1986	24	65	98.81	96.77
121	1871	1860	11	3	99.41	99.84
122	2477	2475	2	0	99.92	100.00
123	1518	1518	0	0	100.00	100.00
124	1602	1598	4	10	99.75	99.38
200	2599	2597	2	2	99.92	99.92
201	1963	1936	27	27	98.62	98.62
202	2135	2131	4	18	99.81	99.16
203	2982	2888	94	124	96.85	95.84
205	2657	2629	28	14	98.95	99.47
207	1862	1850	12	17	99.36	99.09
208	2952	2920	32	32	98.92	98.92
209	3051	3005	46	0	98.49	100.00
210	2645	2605	40	39	98.49	98.53
212	2761	2761	0	0	100.00	100.00
213	3245	3244	1	0	99.97	100.00
214	2273	2251	22	17	99.03	99.25
215	3398	3360	38	1	98.88	99.97
217	2270	2204	66	9	97.09	99.60
219	2154	2154	0	0	100.00	100.00
220	2068	2048	20	0	99.03	100.00
221	2447	2421	26	14	98.94	99.43
222	2624	2606	18	8	99.31	99.70
223	2636	2598	38	5	98.56	99.81
228	2116	2041	75	24	96.46	98.87
230	2257	2257	0	0	100.00	100.00
231	1569	1569	0	0	100.00	100.00
232	1734	1730	4	6	99.77	99.65
233	3074	3074	0	0	100.00	100.00
234	2763	2753	10	0	99.64	100.00
Total	110008	109254	748	610	99.32	99.45

SNRs (Fig.8b, c), all the algorithms are able to get clear QRS complex features. With the decreasing of SNRs, the QRS complexes become less obvious. When the SNR is 0 dB (Fig.8d), the QRS complexes are ruined by noise. In this case, the results of the box-scoring calculation and Pan and Tompkins algorithm give better results than that of phase portraits area calculation.

#### C. Simulated Results of MIT/BIH Arrhythmia Database

The MIT/BIH arrhythmia database is used to evaluate the performance of the proposed box-scoring QRS complex detection algorithm. The detail results are given in Table I. 748 false negative (FN) beats (99.32% sensitivity) and

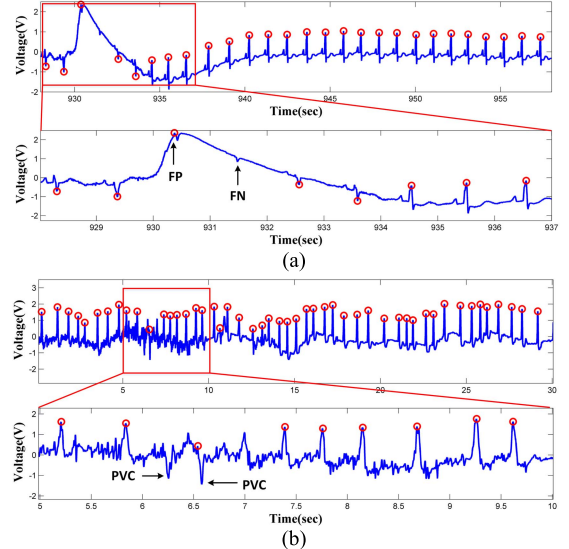


Fig. 9. QRS complex detection results. (a) No.108: severe time-varying morphological changes. (b) No.203: premature ventricular contraction (PVC).

610 false positive (FP) beats (99.45% predictivity) are obtained. The baseline wander, muscle artifacts and the change of the QRS morphological exist in some recordings, such as No.105, No.108, No.201 and No.203. Table II compares the QRS detection results of these recordings by different methods [10], [16]–[18]. It can be seen that for No.108, similar results are obtained by our methods and area calculation [17], [18]. This is reasonable because the operational principle of our algorithm is similar to the area calculation method. As shown in Fig.9a, the FPs and FNs are mainly caused by severe time-varying morphological changes. However, for some other noisy recordings, more false detections obtained. Taking No.203 as an example (Fig.9b), miss detection occurs because the waveforms of the Premature Ventricular Contraction (PVCs) are different from the normal QRS complexes, indicating that our algorithm is sensitive to the shape of R-waves.

Table III gives a summary of the algorithms [10]–[13], [15]–[18] with MIT/BIH arrhythmia database. The calculation is performed on MATLAB (OS: Windows 7, CPU: intel-i7 6700, Memory size: 16GB). All the algorithms are programmed and run in the same environment. The computing time is obtained by running the full 48 recordings. The “-” indicates that the corresponding method is not programmed by us and the data are quoted from the references. It can be seen that the detection accuracy of our algorithm is in the range of other previous works. The main advantage is that our algorithm runs faster than other methods.

#### D. Experimental Results With Microcontroller-Based System

Experiments are carried out with a real-time ECG signal acquisition system developed in our lab (Fig.10a). The ECG signals are differentially amplified by the signal acquisition circuit. After the band-pass filter (passband frequency is 0.3–40 Hz [28], [29]) and notch filter (center frequency is 50Hz), the filtered ECG signal is sampled and converted

TABLE II  
QRS COMPLEX DETECTION RESULTS WITH LOW QUALITY ECG SIGNALS

REC	Our work overall error: 3.80%			Area calculation [17, 18] overall error: 1.88%			Pan and Tompkins [10] overall error: 4.34%			Quadratic filter [16] overall error: 1.89%		
	Total	FP+FN	Error (%)	Total	FP+FN	Error (%)	Total	FP+FN	Error (%)	Total	FP+FN	Error (%)
105	2578	61	2.73	2572	45	1.75	2572	89	3.46	2572	39	1.52
108	1763	20	1.13	1763	20	1.13	1763	221	12.54	1763	72	4.08
201	1963	54	2.75	1963	27	1.38	1963	10	0.51	1963	7	0.36
203	2982	218	7.31	2980	82	2.75	2982	83	2.78	2980	57	1.91

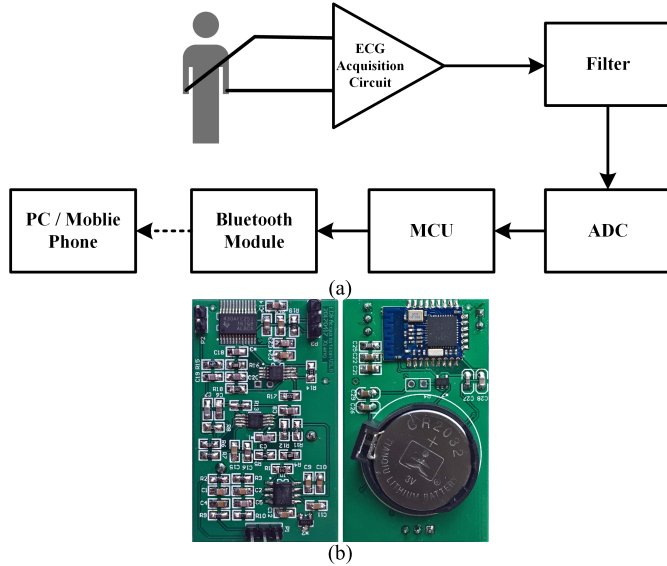


Fig. 10. ECG signal acquisition system. (a) Schematic of the system. (b) The top side of the circuit (left). The bottom side of the circuit (right).

TABLE III  
QRS COMPLEX DETECTION PERFORMANCE COMPARED TO OTHER ALGORITHMS WITH THE MIT/BIH ARRHYTHMIA DATABASE

Methods	Se(%)	P(%)	Computing Time (s)
Our work	99.32	99.45	9.463±0.262
Area calculation [17, 18]	99.82	99.82	97.095±1.077
Pan and Tompkins [10]	99.76	99.56	16.563±0.137
Modified Pan and Tompkins [12]	99.54	99.74	11.208±0.129
Ghaffari [13]	99.91	99.72	153.289±0.833
Quadratic filter [16]	99.82	99.81	-
Sahoo [15]	99.71	99.72	-
Adnane [11]	99.77	99.64	-

to digital time series by the ADC (250Hz sampling frequency, 12-bits resolution). The QRS complexes are locally detected by the proposed method in the microcontroller unit (MCU: MSP430AFE253, Clock Frequency: 1.15MHz, RAM: 0.5KB). The processed ECG signal, as well as QRS complex detection results, are transferred to a smart mobilephone or a PC via Bluetooth. Fig.10b shows photographs of the circuits. The circuits are powered by a 3V lithium coin battery (CR2032).

TABLE IV  
THE COMPUTING TIME OF THE QRS COMPLEX DETECTION ALGORITHMS IN MCU

Methods	Computing Time (ms)	Standard Deviation
Our work	0.583	0.0027
Area calculation [17, 18]	1.030	0.0011
Pan and Tompkins [10]	1.180	0.0001
Modified Pan and Tompkins [12]	0.617	0.0028

The box-scoring calculation algorithm, area calculation [17], [18], Pan and Tompkins [10] and a modified algorithm of Pan and Tompkins proposed by Gutiérrez-Rivas *et al.* [12] are implemented respectively on MCU. The reason for choosing these algorithms is its low computational burden and can work in real-time mode. As mentioned above, the main advantage of our algorithm is its computational complexity. In case of the polygon area calculation formula,  $2n$  multiplications and  $2n - 1$  additions/subtractions are required to perform Eq.1. On the other hand, the box-scoring calculation by Eq.5 only needs  $2n - 1$  additions/subtractions and does not need any multiplication. Therefore, the computational cost is significantly decreased and more suitable to be implemented in MCU.

The operation time is evaluated by simulated signals. The signal generator (Tektronix AFG3021B) is used to generate the simulated ECG signals (normal beat, 60bpm). The simulated ECG signal is sampled and processed real-timely (i.e. signal are processed sample by sample, with no use of global buffers). The processing time for 20 feature points is recorded by the Timer in MCU. After dozens of repetitions, the averaged running time is given in Table IV. It is about two times faster as the area calculation algorithm and the Pan and Tompkins, and about ten percent faster than Modified Pan and Tompkins. It should be noted that the results of the area calculation algorithm gives better performance in MCU based environments than that in MATLAB. This may be caused by the fact that the internal operation of MATLAB is quite different from that of C-coded program in MCU. Another reason is that the results of Table IV are obtained in real-time mode. But in MATLAB, the algorithms are operated in offline mode.

Twenty-three volunteers (3 women and 20 men, ranged from 21-60 years of age) are experimentally tested by the

TABLE V  
RESULTS OF THE BOX-SCORING QRS COMPLEX DETECTION ALGORITHM USING MEASURED DATA

Sub.	Total	TP	FN	FP	Se(%)	P(%)
No.1	82	81	1	1	98.78	98.78
No.2	63	63	0	0	100.00	100.00
No.3	68	68	0	0	100.00	100.00
No.4	79	76	3	2	96.20	97.44
No.5	87	84	3	3	96.55	96.55
No.6	89	88	1	1	98.88	98.88
No.7	85	72	10	9	87.80	88.89
No.8	90	79	8	4	90.80	95.18
No.9	95	82	13	6	86.32	93.18
No.10	87	86	1	1	98.85	98.85
No.11	103	102	1	0	99.03	100.00
No.12	84	83	1	0	98.81	100.00
No.13	71	71	0	0	100.00	100.00
No.14	69	57	12	12	82.61	82.61
No.15	74	74	0	0	100.00	100.00
No.16	84	84	0	0	100.00	100.00
No.17	98	95	3	1	96.94	98.96
No.18	73	71	2	1	97.26	98.61
No.19	83	79	4	4	95.18	95.18
No.20	73	73	0	0	100.00	100.00
No.21	90	88	2	1	97.78	98.88
No.22	80	80	0	0	100.00	100.00
No.23	83	83	0	0	100.00	100.00
Total	1890	1819	65	46	96.55	97.53

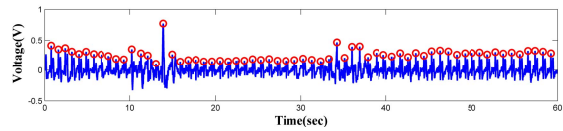


Fig. 11. QRS complex detection results during the Valsalva maneuver (volunteer No.2).

real-time ECG signal acquisition system. No volunteer reported any difficulties or discomfort during experiments. Part of these people had done physical labor before experiment, and all the subjects were asked to sit still when measuring the ECG data by our device (one minute, dry electrodes, Hand-ECG). All the acquired ECG signals are recorded and manually annotated to be used as reference. The detail results of our algorithm are given in Table V. The algorithm obtains sensitivity of 96.55% and predictivity of 97.53%. The measurement results are slightly lower than the simulation results. This is because the measurement time is only one minute, and the signal quality of the dry electrodes is lower than the Ag/AgCl electrodes. Anyway, such a measurement reliability should be adequate for daily life and health care applications [7].

Another experiments are carried out by measuring the ECG signals with two devices at the same time. One is our real-time ECG signal acquisition system, another is the clinical ECG instrument (SE-601B, EDAN Instruments, Shenzhen, China). All volunteers have prior experience with the Valsalva maneuver (VM) [30]. In the experiments, five volunteers are asked to do a VM within one minute, and the QRS complexes are detected. As an example, the QRS complex detection results of a volunteer (No.2, male, age: 31, height: 176cm, weight: 78Kg) are shown in Fig.11. The heart rates calculated

TABLE VI  
HEART RATES RESULTS

Sub.	Our Device MeanHR ± SD (bpm)	ECG Instrument MeanHR ± SD (bpm)	Error Rate (%)
No.1	75.0±5.6	75.8±5.9	2.9%
No.2	62.8±3.4	64.2±5.8	3.6%
No.3	63.0±4.1	63.8±3.5	2.3%
No.4	72.0±5.8	71.8±5.2	0.7%
No.5	67.3±2.3	67.8±2.5	2.2%

from all the five volunteers are listed in Table VI. The tested results obtained by the clinical ECG instrument are used as the reference. As shown in Table VI, the maximum error rate is only 3.6%.

#### IV. CONCLUSION

Based on the phase space reconstruction and gridding partition, a box-scoring calculation method is proposed for QRS complex detection. The performance of the proposed algorithm is evaluated by the MIT-BIH Arrhythmia Database and the measured ECG signals acquired by our real-time ECG signal acquisition system. The main advantage of the algorithm is the lower computational complexity. The algorithm can be further applied to various wearable ECG acquisition devices.

#### REFERENCES

- [1] H. Lee, H. Ko, C. Jeong, and J. Lee, "Wearable photoplethysmographic sensor based on different LED light intensities," *IEEE Sensors J.*, vol. 17, no. 3, pp. 587–588, Feb. 2017.
- [2] B. Yang, C. Yu, and Y. Dong, "Capacitively coupled electrocardiogram measuring system and noise reduction by singular spectrum analysis," *IEEE Sensors J.*, vol. 16, no. 10, pp. 3802–3810, May 2016.
- [3] T. Liang and Y. J. Yuan, "Wearable medical monitoring systems based on wireless networks: A review," *IEEE Sensors J.*, vol. 16, no. 23, pp. 8186–8199, Dec. 2016.
- [4] D. P. Tobón, S. Jayaraman, and T. H. Falk, "Improved heart rate variability measurement based on modulation spectral processing of noisy electrocardiogram signals," in *Proc. IEEE 14th Int. Conf. Wearable Implant. Body Sensor Netw. (BSN)*, May 2017, pp. 51–54.
- [5] K. K. Tsoi *et al.*, "Personal wearable devices to measure heart rate variability: A framework of cloud platform for public health research," in *Proc. Int. Conf. Digit. Health (DH)*, 2017, pp. 207–208.
- [6] E. S. Kaappa, A. S. Joutsen, and J. Vanhala, "Performance analysis of novel flexible electrodes for wearable ECG/heart rate monitoring," in *Proc. Eur. Med. Biol. Eng. Conf. Nordic-Baltic Conf. Biomed. Eng. Med. Phys.*, vol. 65, 2017, pp. 237–240.
- [7] M. M. Baig, H. GholamHosseini, A. A. Moqeeem, F. Mirza, and M. Lindén, "A systematic review of wearable patient monitoring systems—Current challenges and opportunities for clinical adoption," *J. Med. Syst.*, vol. 41, p. 115, Jul. 2017.
- [8] S. Krachunov *et al.*, "Energy efficient heart rate sensing using a painted electrode ECG wearable," in *Proc. Global Internet Things Summit (GIoTS)*, Jun. 2017, pp. 1–6.
- [9] R. J. Martis, U. R. Acharya, and H. Adeli, "Current methods in electrocardiogram characterization," *Comput. Biol. Med.*, vol. 48, pp. 133–149, May 2014.
- [10] J. Pan and W. J. Tompkins, "A real-time QRS detection algorithm," *IEEE Trans. Biomed. Eng.*, vol. BME-32, no. 3, pp. 230–236, Mar. 1985.
- [11] M. Adnane, Z. W. Jiang, and S. Choi, "Development of QRS detection algorithm designed for wearable cardiorespiratory system," *Comput. Methods Programs Biomed.*, vol. 93, no. 1, pp. 20–31, 2009.
- [12] R. Gutiérrez-Rivas, J. J. García, W. P. Marnane, and Á. Hernández, "Novel real-time low-complexity QRS complex detector based on adaptive thresholding," *IEEE Sensors J.*, vol. 15, no. 10, pp. 6036–6043, Oct. 2015.

- [13] A. Ghaffari, H. Golbayani, and M. Ghasemi, "A new mathematical based QRS detector using continuous wavelet transform," *Comput. Electr. Eng.*, vol. 34, no. 2, pp. 81–91, 2008.
- [14] R. R. Jorge *et al.*, "Adaptive threshold, wavelet and Hilbert transform for QRS detection in electrocardiogram signals," in *Proc. Int. Conf. P2P, Parallel, Grid, Cloud Internet Comput.*, Nov. 2017, pp. 777–786.
- [15] S. Sahoo, P. Biswal, T. Das, and S. Sabut, "De-noising of ECG Signal and QRS detection using Hilbert transform and adaptive thresholding," *Proc. Technol.*, vol. 25, pp. 68–75, Jan. 2016.
- [16] P. Phukpattaranont, "QRS detection algorithm based on the quadratic filter," *Expert Syst. Appl.*, vol. 42, no. 11, pp. 4867–4877, 2015.
- [17] J. W. Lee, K.-S. Kim, B. Lee, B. Lee, and M.-H. Lee, "A real time QRS detection using delay-coordinate mapping for the microcontroller implementation," *Ann. Biomed. Eng.*, vol. 30, no. 9, pp. 1140–1151, 2002.
- [18] M. Cvikel, F. Jager, and A. Zemva, "Hardware implementation of a modified delay-coordinate mapping-based QRS complex detection algorithm," *EURASIP J. Adv. Signal Process.*, vol. 2007, no. 1, p. 104, 2007.
- [19] A. Amann, R. Tratnig, and K. Unterkofler, "Detecting ventricular fibrillation by time-delay methods," *IEEE Trans. Biomed. Eng.*, vol. 54, no. 1, pp. 174–177, Jan. 2007.
- [20] R. R. Sarvestani, R. Boostani, and M. Roopaei, "VT and VF classification using trajectory analysis," *Nonlinear Anal., Theory Methods Appl.*, vol. 71, no. 12, pp. 55–e61, 2009.
- [21] M. Roopaei, R. Boostani, R. R. Sarvestani, M. A. Taghavi, and Z. Azimifar, "Chaotic based reconstructed phase space features for detecting ventricular fibrillation," *Biomed. Signal Process. Control*, vol. 5, no. 4, pp. 318–327, 2010.
- [22] F. Takens, "Detecting strange attractors in turbulence," in *Dynamical Systems and Turbulence*. Berlin, Germany: Springer, 1981.
- [23] T. D. Sauer, J. A. Yorke, and M. Casdagli, "Embedology," *J. Statist. Phys.*, vol. 65, nos. 3–4, pp. 579–616, Nov. 1991.
- [24] J. M. Moore, M. Small, and A. Karrech, "Improvements to local projective noise reduction through higher order and multiscale refinements," *Chaos*, vol. 25, no. 6, p. 063114, 2015.
- [25] W. Liebert, K. Pawelzik, and H. G. Schuster, "Optimal embeddings of chaotic attractors from topological considerations," *Europhys. Lett.*, vol. 14, no. 6, pp. 521–526, 1991.
- [26] A. M. Fraser and H. L. Swinney, "Independent coordinates for strange attractors from mutual information," *Phys. Rev. A, Gen. Phys.*, vol. 33, no. 2, pp. 1134–1140, Feb. 1986.
- [27] G. B. Moody and R. G. Mark, "The impact of the MIT-BIH arrhythmia database," *IEEE Eng. Med. Biol. Mag.*, vol. 20, no. 3, pp. 45–50, May/Jun. 2001.
- [28] U. R. Acharya *et al.*, *Advances in Cardiac Signal Processing*. Berlin, Germany: Springer, 2007.
- [29] I. Christov, T. Neycheva, R. Schmid, T. Stoyanov, and R. Abächerli, "Pseudo-real-time low-pass filter in ECG, self-adjustable to the frequency spectra of the waves," *Med. Biol. Eng. Comput.*, vol. 55, no. 9, pp. 1579–1588, 2017.
- [30] A. Pandya and E. Lang, "Valsalva maneuver for termination of supraventricular tachycardia," *Ann. Emergency Med.*, vol. 65, no. 1, pp. 27–29, 2015.

**Zhongjie Hou** was born in Hunan, China, in 1990. He received the M.Sc. degree from the Department of Automation, Tsinghua University, in 2015, where he is currently pursuing the Ph.D. degree. His main research interest is biological signal measuring and processing.

**Yonggui Dong** received the B.S. degree in mechanical engineering and the Ph.D. degree in mechatronics from Tsinghua University, Beijing, China, in 1988 and 1994, respectively. He is currently a Professor and a Ph.D. Supervisor with the Department of Precision Instruments, Tsinghua University. His current research interests include sensor technology, measurement and test technology, and intelligent instruments technology.

**Jinxi Xiang** was born in Guangdong, China, 1994. He received the B.Sc. degree from Wuhan University, in 2016. He is currently pursuing the Ph.D. degree with Tsinghua University. His main research interest is human body character signal measuring.

**Xuewu Li** was born in Gansu, China, 1988. He is currently pursuing the M.Sc. degree with the School of Mechanical, Electronic and Control Engineering, Beijing Jiaotong University. His main research interest is vibration signal measuring.

**Bin Yang** was born in Shanxi, China, in 1990. He received the B.Sc. degree from the Harbin Institute of Technology, in 2012. He is currently pursuing the Ph.D. degree with Tsinghua University. His main research interest is human body character signal measuring.